

# Theory of Fano effects in an Aharonov-Bohm ring with a quantum dot

Takeshi Nakanishi and Kiyoyuki Terakura

*National Institute of Advanced Industrial Science and Technology, 1 Umezono, Tsukuba 305-8568, Japan*

Tsuneya Ando

*Department of Physics, Tokyo Institute of Technology, 2-12-1 Ookayama, Meguro-ku, Tokyo 152-8551, Japan*

(Received 15 October 2003; published 10 March 2004)

Using a realistic model of a quantum dot embedded in an Aharonov-Bohm ring with several current-carrying channels, we demonstrate phase persistence in the Fano and Aharonov-Bohm effects as has been observed in experiments. The phase persistence arises because most of the states contributing to the Coulomb oscillation of the conductance are weakly coupled to ring states through a small number of states giving a major contribution to the conductance under off-resonant conditions.

DOI: 10.1103/PhysRevB.69.115307

PACS number(s): 73.63.Kv, 73.23.Hk, 75.47.Jn

## I. INTRODUCTION

In an Aharonov-Bohm (AB) ring containing a quantum dot, a series of consecutive conductance peaks with a Fano-type interference with similar asymmetry and phase of an AB oscillation have been observed.<sup>1,2</sup> A Fano-type line shape was reported also in a weakly coupled single quantum dot.<sup>3,4</sup> The purpose of this work is to theoretically study Fano resonances in a realistic AB ring with a quantum dot and to understand some of the interesting experimental findings.

Fano proposed a theory on effects of configuration interaction on intensities and phase shifts, in which interference of a localized state with a continuum was shown to give rise to asymmetric peaks in excitation spectra.<sup>5</sup> The Fano effect has been studied mainly in optical absorption spectra of impurities in solids, in which the Fano line shape is known to be observed easily particularly when a direct excitation from a ground state to a localized state is forbidden.<sup>6,7</sup>

In earlier experiments, AB oscillations were observed in an AB ring with a quantum dot and the phase of the oscillation was shown to change by  $\pi$  across a resonance peak.<sup>8-10</sup> A surprising and unexpected finding is that the phase becomes the same between adjacent peaks, showing that it has to change by another  $\pi$  between those peaks. Since then, various theoretical studies have been reported on the phase of the AB oscillation and the Fano effect within one-dimensional (1D) models in which the AB ring consists of a chain.<sup>11-18</sup>

It was suggested, for example, that because the Friedel sum rule leading to a  $\pi$  change across a peak is still valid in the presence of a Fano-type interference, the extra  $\pi$  change between neighboring peaks is likely to be due to hidden electron charging events that do not cause conductance peaks.<sup>12</sup> The possible disappearance of some peaks due to an interference inside the AB ring<sup>13</sup> and the vanishing of the transmission coefficient occurring in a 1D model due to the Fano-type interference<sup>16</sup> were suggested as possible candidates for the mechanism giving rise to such an extra phase change.

Since the more recent observation of a clear Fano effect,<sup>1</sup> various 1D model calculations were further made. For example, an alternating sign change of a Fano parameter char-

acterizing the asymmetry was obtained.<sup>17</sup> Effects of dephasing were studied.<sup>18</sup>

In this work, with the use of a realistic model we shall provide a convincing explanation of the phase persistence in the AB and Fano effects observed experimentally. The model AB ring contains several conducting channels and a quantum dot with dimensions comparable to those in the experiments. The organization of the paper is as follows: After introducing the realistic model in Sec. II, numerical results are shown in Sec. III in the case where double-slit conditions are valid approximately. Coexistence of strongly and weakly coupled states in the dot with finite width is proposed to understand the numerical results. Numerical results in more general cases are presented in Sec. IV. Discussion on the relation to experiments is given in Sec. V and a summary and conclusion are given in Sec. VI.

## II. MODEL AND METHOD

We use a model of the AB ring with radius  $a$ , straight up and down arms with length  $L$ , a quantum dot with length  $L_D$  in the down arm separated by wall barriers with length  $L_W$ , and a control gate with length  $L_W$  as shown in Fig. 1. The strength of a magnetic field applied perpendicular to the AB ring is characterized by  $\phi/\phi_0$ , where  $\phi$  is magnetic flux passing through the stadium with area  $aL + \pi a^2/4$  and  $\phi_0$  is the magnetic flux quantum given by  $\phi_0 = ch/e$ .

To construct the model potential, we first consider a hexagon defined by six vertices at  $\mathbf{r} = \pm \mathbf{a}/2$ ,  $\pm \mathbf{b}/2$ , and  $\pm (\mathbf{a} - \mathbf{b})/2$  with  $\mathbf{a} = (\sqrt{3}/2, 1/2)a$  and  $\mathbf{b} = (0, 1)a$  and define an antidot potential which vanishes outside the hexagon and is given by

$$u_{\text{antidot}}(\mathbf{r}) = u_0 \left| \cos\left(\frac{\pi \mathbf{a} \cdot \mathbf{r}}{a^2}\right) \cos\left(\frac{\pi \mathbf{b} \cdot \mathbf{r}}{a^2}\right) \cos\left(\frac{\pi (\mathbf{a} - \mathbf{b}) \cdot \mathbf{r}}{a^2}\right) \right|^{4/3}, \quad (1)$$

inside the hexagon. This potential was used in previous studies on transport properties of antidot lattices.<sup>19</sup>

We consider next the rectangular region near the top-right corner as shown in Fig. 1 and define the origin  $\mathbf{r} = 0$  at the bottom-left corner. The rectangle is divided into four differ-

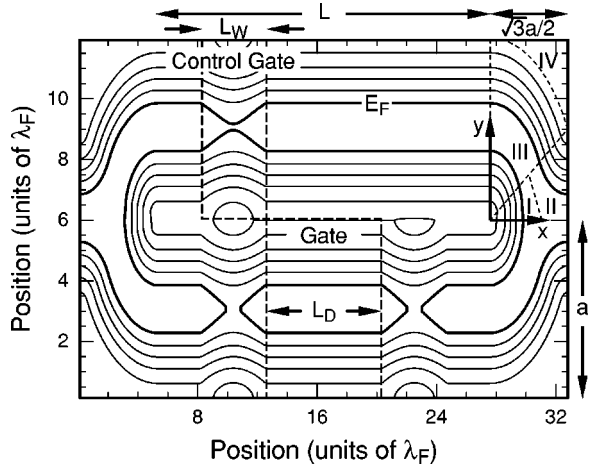


FIG. 1. Equipotential lines of the model AB ring with a dot, plotted with energy interval of Fermi energy  $E_F$ . The thick lines correspond to the Fermi energy. The gate potential  $V_g$  and the control gate potential  $V_c$  are applied in the dashed rectangular regions with width  $L_W$  and  $L_D$ , respectively. In this example  $V_g/E_F=0$ ,  $V_c/E_F=0.95$ , and  $W/E_F=1.03$ . The rectangular region near the top-right corner is separated into four regions I, II, III, and IV.

ent regions denoted by I, II, III, and IV by dashed lines. The region I is defined by  $y < x/\sqrt{3}$  and  $y < -\sqrt{3}x + a$ , the region II is defined by  $y < x/\sqrt{3}$  and  $y > -\sqrt{3}x + a$ , and the region IV is defined by  $\sqrt{x^2 + y^2} > 2a$ . The potential is defined by  $v(\mathbf{r}) = v_{\text{antidot}}(\mathbf{r})$  in I,  $v(\mathbf{r}) = v_{\text{antidot}}(\mathbf{r} - \mathbf{a})$  in II, and  $v(\mathbf{r}) = u_0$  in region IV. In region III the potential along the line  $y = x/\sqrt{3}$  of the regions I and II is rotated around the origin. The potential in the up arm is the same as that along  $x=0$  of the region III. The potential in the rectangular regions near other corners and in the down arm are defined in a symmetric way. Two ideal leads with a uniform cross section same as that in the up and down arms are continuously connected to the left and right entrances of the AB ring.

The wall potential separating the dot from the arm is defined as

$$V(\mathbf{r}) = W \cos\left(\frac{\pi x}{L_W}\right) \quad (2)$$

for  $-L_W/2 < x < L_W/2$  and  $-a < y < 0$ , where an origin of  $x$  is chosen at the center of each wall. The potential of the control gate is given by the same expression for  $-L_W/2 < x < L_W/2$  and  $0 < y < a$  except that the height  $W$  is replaced by  $V_c$ . They are superposed on the potential of the AB ring. A gate potential  $V_g$  is uniformly applied in the dot in the region of  $-a < y < 0$  with length  $L_D$  which is shown by dashed rectangular region in Fig. 1.

For a realistic quantum dot embedded in the AB ring, the adiabatic conditions are satisfied, i.e.,  $|dD(x)/dx| \ll 1$  and  $|D(x)d^2D(x)/dx^2| \ll 1$  with  $D(x)$  being the width of the waveguide at the Fermi energy  $E_F$ . Therefore, we choose  $L_W/\lambda_F = 5$  with Fermi wavelength  $\lambda_F$ . Calculations of transmission and reflection probabilities for the single wall with height  $W \lesssim E_F$  reveal that essentially electrons in the lowest 1D subband with the highest velocity in the incident

direction can get over the wall and there is very little mixing between different 1D subbands or channels. In order to simulate actual situations, further, we introduce a weak random potential in the dot. The amount of the disorder corresponds to a mean-free path of  $10 \times \lambda_F$  or level broadening of  $0.015E_F$  in the two-dimensional system.

We use some fixed parameters in numerical calculations,  $W/E_F = 1.03$ , the ring radius  $a/\lambda_F = 6$ , the arm length  $L/\lambda_F = 20.8$ , and the width of arms and leads  $1.8\lambda_F$  at the Fermi energy, which results in  $u_0/E_F = 5.44$ . In comparison with the geometry of the actual experiments for which  $\lambda_F = 40$  nm,<sup>1</sup> the system size is roughly half except for  $L_D$  of a comparable length. There are three sets of the traveling modes in the arms and leads, which can describe the actual feature of the experiment in which there are several channels. Further, we shall consider the magnetic flux around  $\phi/\phi_0 = 80$  corresponding to 1.3 T, which is typical magnetic field in the experiments.

A self-consistent calculation in quantum wires fabricated at GaAs/AlGaAs heterostructures suggests that the potential is nearly parabolic for a wire with small width, but consists of a flat central region and a parabolic increase near the edge for a wider wire.<sup>20,21</sup> In the above the exponent  $4/3$  in  $v_{\text{antidot}}(\mathbf{r})$  has been chosen in such a way that the total exponent of cosine function becomes four, for which the potential gradient at the Fermi energy corresponds to that of such a realistic confinement potential. The model is essentially the same as that described in a previous study apart from the presence of the dot and the control gate.<sup>19</sup>

The conductance is calculated by the use of the Landauer formula

$$G = \frac{e^2}{\pi\hbar} \sum_{jj'} |t_{jj'}|^2, \quad (3)$$

where  $t_{jj'}$  is the transmission coefficient for a wave incoming from the  $j'$ th channel in the left lead and outgoing to the  $j$ th channel in the right.<sup>22</sup> The summation is taken over all traveling modes in the leads. To calculate  $t_{jj'}$ , we use recursive Green's function technique on the lattice model with a lattice constant  $a'$ .<sup>23</sup> For explicit numerical calculations we choose  $\lambda_F/a' = 7$ .

### III. DOUBLE-SLIT REGIME

In this section we consider the case where the up arm is nearly pinched off by the control gate. In this case the situation is close to that of so-called double slit experiments, because the transmission probability of an electron passing through the up arm is small and not so much different from that through the down arm and therefore multiple scattering in the AB ring is less important.

Figure 2 shows an example of the calculated conductance as a function of the gate potential for the control gate  $V_c/E_F = 1$ . Figure 2(a) for  $\phi/\phi_0 = 79.9$  and Fig. 2(b) for  $\phi/\phi_0 = 80.5$  correspond to a maximum and minimum of the AB oscillation of the conductance away from the peak region, i.e., under off-resonant conditions. Figure 2(c) shows

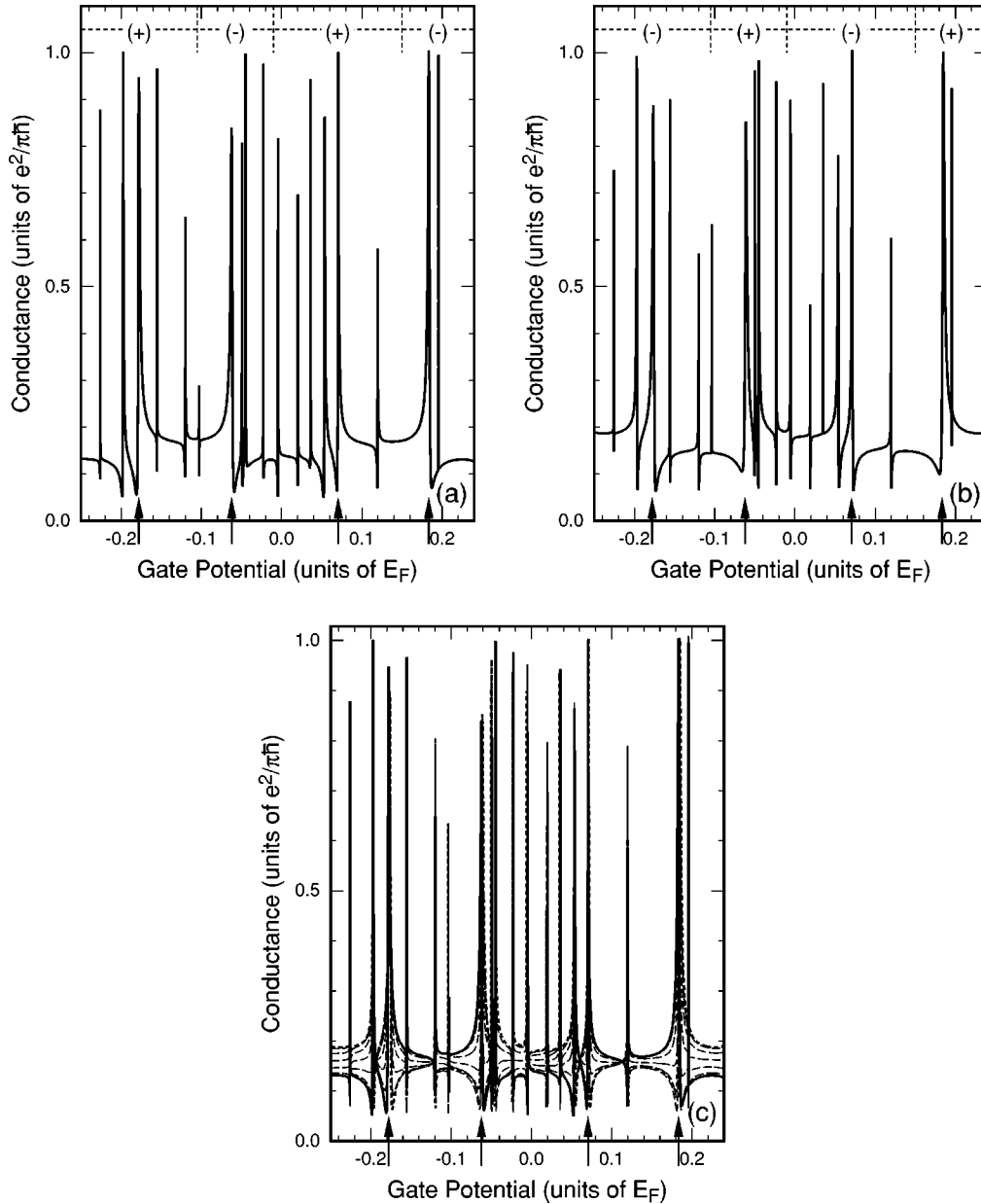


FIG. 2. Fano resonances in the calculated conductance at both wide and narrow peaks for flux (a)  $\phi/\phi_0=79.9$  and (b)  $\phi/\phi_0=80.5$ . (c) The conductance, when the applied magnetic flux is shifted finely at regular intervals from  $\phi/\phi_0=79.9$  to  $\phi/\phi_0=80.5$  (the solid line for  $\phi/\phi_0=79.9$ , the dotted line  $\phi/\phi_0=80.5$ , the thin dashed lines in between). The arrows indicate the position of the wide peaks when the up arm is pinched off. In (a) and (b) the region for positive and negative values of the asymmetry parameter  $q'$  are also shown by (+) and (-), respectively.

the conductances for intermediate flux values with a regular interval by thin dashed lines.

Many peaks appear in the conductance, but they can be classified into two groups, small numbers of wide peaks with large broadening and large numbers of narrow peaks. In this example, the wide peaks are at  $V_g/E_F = -0.18, -0.06, 0.07,$  and  $0.18$  indicated by arrows in the figures. All resonance peaks in the conductance are asymmetric with a dip in the right or left side. This asymmetry is due to interference of the waves passing through the up arm and transmitted resonantly through the dot in the down arm, i.e., the so-called Fano interference.

In order to analyze such interference effects including the AB oscillation, we first consider transmission coefficients  $t_{jj'}^d$ , through a quantum dot embedded in a straight waveguide. In the vicinity of a dot level with energy  $E_\nu$ , the transmission coefficient through the dot is given by

$$t_{jj'}^d = \frac{-2\pi i V_{j\nu}(E) V_{\nu j'}(E) D(E)}{E - E_\nu - F_\nu + i\Gamma_\nu}, \quad (4)$$

where  $V_{j\nu}(E)$  and  $V_{\nu j'}(E)$  are the matrix elements of transitions from the dot state to the outgoing states and from the

incident to the dot state, respectively,  $D(E)$  is the density of states in each waveguide, and

$$F_\nu = P \int \frac{|V_\nu(E')|^2}{E' - E_\nu} D(E') dE',$$

$$\Gamma_\nu = \pi |V_\nu(E)|^2 D(E), \quad (5)$$

with  $|V_\nu(E')|^2$  being the total intensity of the transition between the dot and the left and right waveguides. This is rewritten as

$$t_{jj'}^d = \frac{\alpha_{jj'}}{\epsilon + i}, \quad (6)$$

with

$$\alpha_{jj'} = -2\pi i V_{j\nu}(E) V_{\nu j'}(E) D(E) \Gamma_\nu^{-1},$$

$$\epsilon = (E - E_\nu - F_\nu) \Gamma_\nu^{-1}. \quad (7)$$

The transmission probabilities exhibit a resonance with the conventional Breit-Wigner lineshape.

When the double-slit condition is valid, the transmission through the AB ring incoming from the  $j'$ th channel in the left lead and outgoing to the  $j$ th channel in the right lead is given by

$$t_{jj'} = t_{jj'}^0 + t_{jj'}^d, \quad (8)$$

where  $t_{jj'}^0$  is a transmission coefficient for the up arm, essentially independent of energy in the energy scale determined by  $\Gamma_\nu$ . Effects of scattering at entrances of the AB ring can be absorbed in the coefficients  $\alpha_{jj'}$  for  $t_{jj'}^d$ . The total transmission probability is written as

$$|t_{jj'}|^2 = |t_{jj'}^0|^2 \frac{|\epsilon + q_{jj'}|^2}{\epsilon^2 + 1}, \quad (9)$$

with a complex Fano parameter

$$q_{jj'} = \frac{\alpha_{jj'}}{t_{jj'}^0} + i. \quad (10)$$

As a result, the total conductance is given by

$$G = \frac{e^2}{\pi\hbar} \sum_{j,j'} |t_{jj'}|^2 = \frac{e^2}{\pi\hbar} T_0 \frac{|\epsilon + q|^2}{\epsilon^2 + 1}, \quad (11)$$

with a complex Fano parameter  $q = q' + iq''$  and a parameter  $T_0$ , which are given by

$$T_0 = \sum_{jj'} |t_{jj'}^0|^2,$$

$$q' = T_0^{-1} \sum_{jj'} |t_{jj'}^0|^2 q'_{jj'},$$

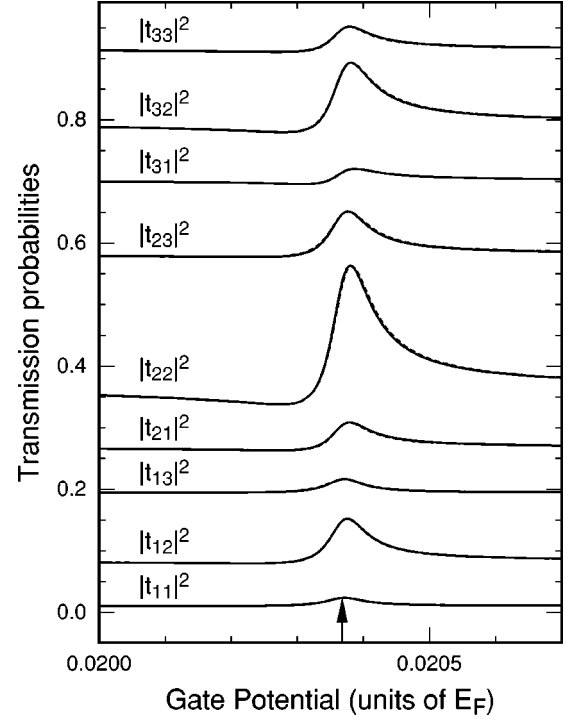


FIG. 3. Calculated transmission probabilities (solid lines) for a narrow peak at  $V_g = 0.02E_F$  of Fig. 2(a) together with fitted results using Eq. (9) given by dotted lines. The origin of the vertical axis is shifted consecutively.  $\phi/\phi_0 = 79.7$ . The common Fano parameters are  $E_0 = 0.020368E_F$  (denoted by arrow) and  $\Gamma/E_F = 7.0 \times 10^{-5}$ .

$$(q'')^2 = T_0^{-1} \sum_{jj'} |t_{jj'}^0|^2 [(q'_{jj'})^2 + (q''_{jj'})^2] - (q')^2. \quad (12)$$

The real part  $q'$  of  $q$  determines the asymmetry of the conductance line shape, i.e., a dip appears in the left-hand side of a peak for positive  $q'$  and in the right-hand side for negative  $q'$ .

Transmission probabilities  $|t_{jj'}|^2$  in the vicinity of the narrow peak at  $V_g/E_F = 0.02$  in Fig. 2(a) are shown in Fig. 3. As shown by dotted lines, the transmission probabilities are well fitted with the Fano line shape given by Eq. (9). Such fitting works quite well for all narrow peaks as well as wide peaks. This means that the double-slit condition is realized quite well.

The asymmetry of the Fano line shape varies as a function of the magnetic flux as can be seen in Fig. 2. Figure 4 shows the explicit magnetic-field dependence of obtained  $q'$  of the narrow peak at  $V_g/E_F = 0.02$ . The Fano parameter shows a clear oscillation, taking positive and negative value, with period  $\phi_0$ . This AB oscillation of  $q'$  is qualitatively in good agreement with the behavior observed experimentally [see Fig. 4(a) of Ref. 1, for example]. Further, Fig. 6(b) of Ref. 2 shows the experimental result of a clear sinusoidal oscillation with an amplitude similar to the present result.

Figure 2 shows also that  $q'$  and correspondingly the phase of the AB oscillation of the wide peaks changes sign alternately when the gate potential crosses them. For the narrow peaks, on the other hand, the sign of  $q'$  does not show such an alternate change from peak to peak but follows the

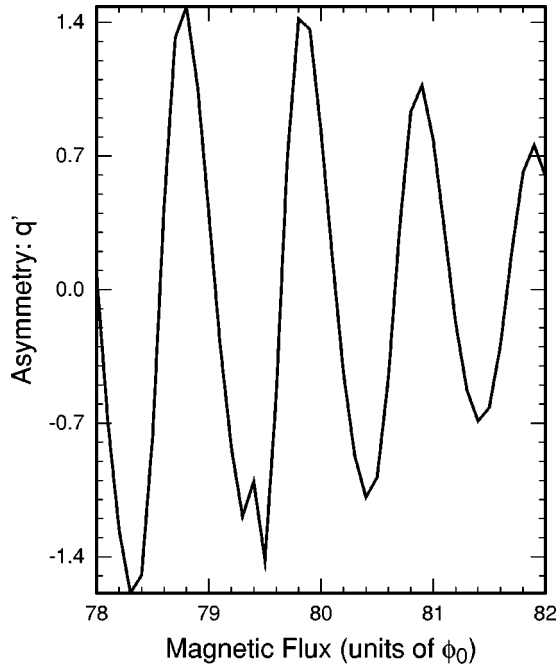


FIG. 4. Calculated AB oscillation of the real part  $q'$  of the Fano parameter  $q$  for the peak shown in Fig. 3.

sign of the nearest wide peaks. In fact, four narrow peaks in the range  $-0.11 < V_g/E_F < -0.01$  have a dip in the right side of peaks, in agreement with the behavior of the wide peak at  $-0.06$ . Further, five narrow peaks in  $-0.01 < V_g/E_F < 0.13$  have a dip in the left side of the peak again

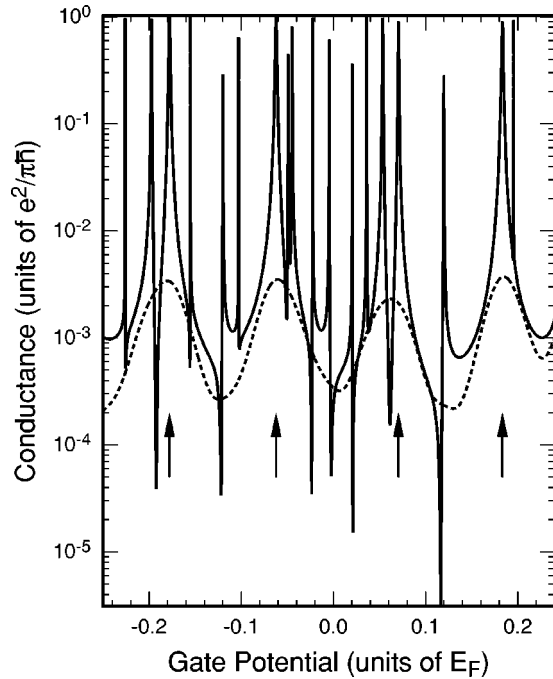


FIG. 5. Resonant peaks in the conductance in the presence of a magnetic field  $\phi/\phi_0=79.9$ , when the control gate is pinched off with  $V_c/E_F=2$ . The conductance averaged over the gate potential with width  $0.01E_F$  is shown by a dotted line. The arrows indicate the position of the wide peaks.

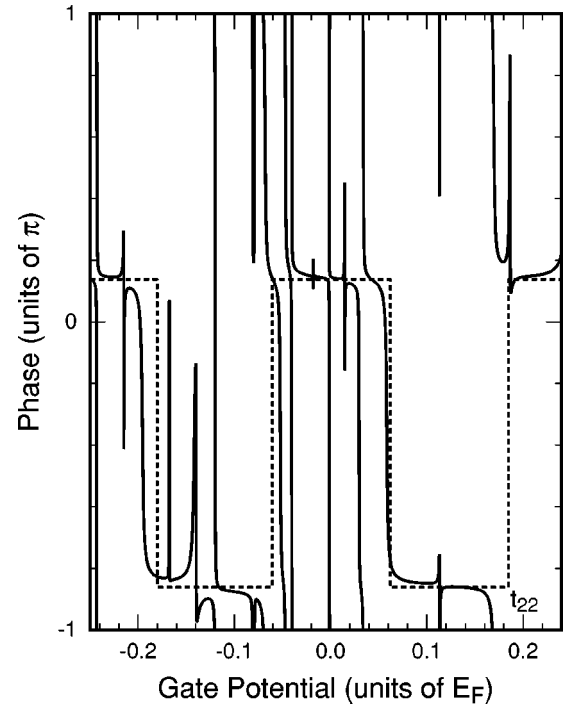


FIG. 6. An example of the phase of calculated  $t_{22}$ . The dotted line is a guide to eyes, which exhibits a discrete jump at the peaks of the dotted line in Fig. 5.

following the nearest wide peak at 0.07. In Figs. 2(a) and 2(b) the sign of  $q'$  of narrow peaks is denoted by (+) and (-).

In a crude approximation, states in the dot can be obtained by discretizing the wave vector along the waveguide direction corresponding to a confinement potential. In this approximation transmissions through dot states with the same 1D subband index are possible and in particular those associated with the lowest subband having the largest kinetic energy in the waveguide direction contribute to transmissions because of the lowest effective tunneling barrier. The wide resonances shown in Fig. 2 actually correspond to such states, which can directly be verified by the wave function in the dot.

This selection rule is violated in the realistic confinement potential and also by the presence of unavoidable disorder. Let  $\hat{H}'$  be the Hamiltonian describing effects of such deviation,  $\psi_n^0$  be a dot state uncoupled to waveguide states in the absence of  $\hat{H}'$ , and  $\psi_N^0$  be the nearest dot state coupled to waveguide states even in the absence of  $\hat{H}'$ . Then, apart from energy shift, the state  $\psi_n$  associated with  $\psi_n^0$  now contains a contribution of  $\psi_N^0$ , i.e.,

$$\psi_n \approx \psi_n^0 + \psi_N^0 \frac{\langle N | \hat{H}' | n \rangle}{E_n - E_N}, \quad (13)$$

where the lowest-order energy shift has been taken into account already in energies  $E_n$  and  $E_N$ . Then, in the vicinity of  $E_n$ , the matrix element for transmission through the dot becomes

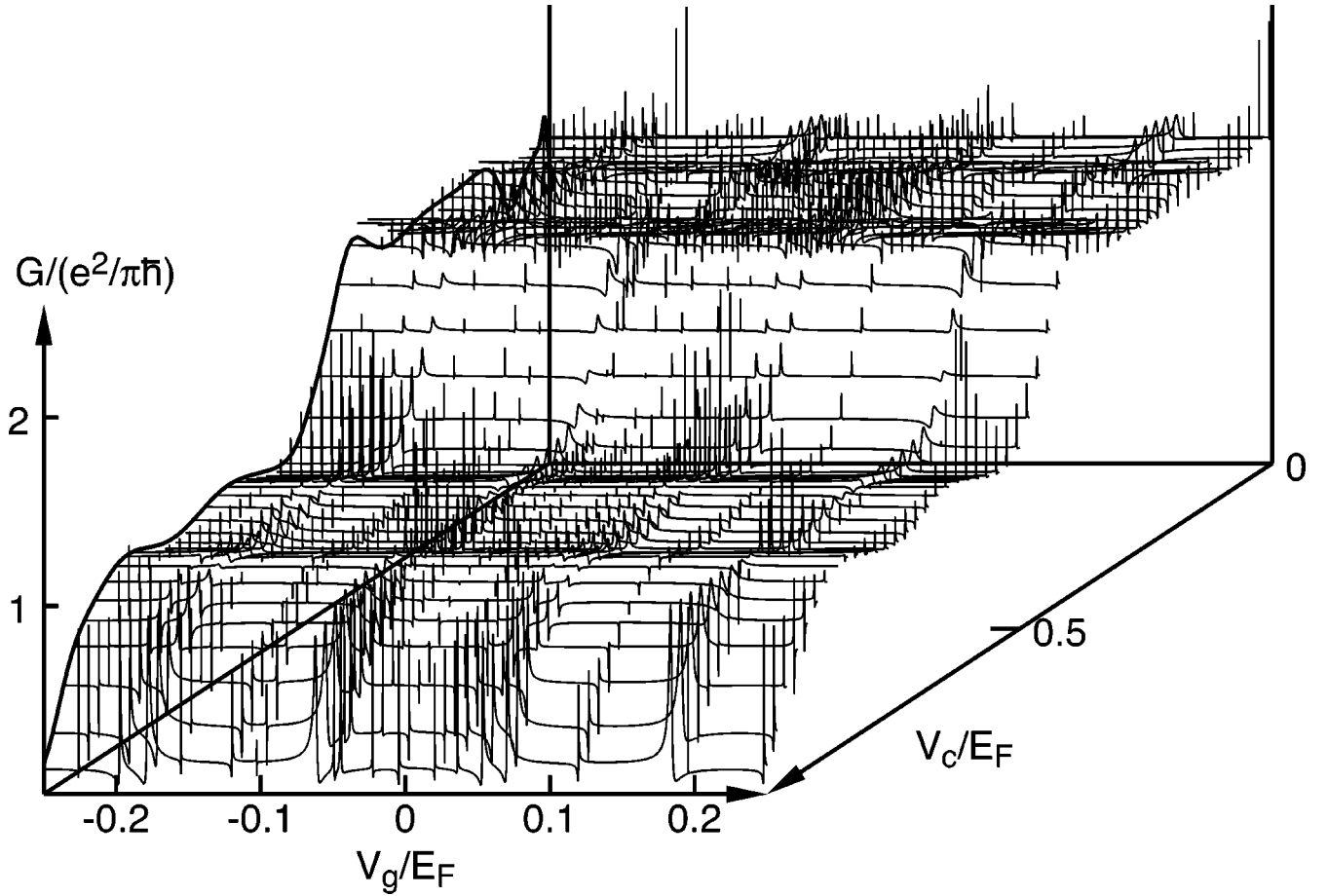


FIG. 7. Calculated conductance for  $-0.25 \leq V_g/E_F \leq 0.25$  and  $0 \leq V_c/E_F \leq 1$ , applying the magnetic flux  $\phi/\phi_0 = 79.9$ .

$$V_{jn}V_{nj'} \approx V_{jN}V_{Nj'} \frac{|(N|\hat{H}'|n)|^2}{(E_n - E_N)^2}. \quad (14)$$

This shows that the phase of  $V_{jn}V_{nj'}$  is given by that of  $V_{jN}V_{Nj'}$  of the nearest wide peak, explaining the essential feature of the numerical result that the asymmetry of the Fano interference of narrow peaks follows that of a neighboring wide peak.

When only the transport through a dot embedded in a waveguide is possible, i.e., when the control gate is pinched off, a Fano-type interference is possible between different processes within a dot. A nonresonant transmission through the dot state  $E_N$  becomes significant, which is ignored in the previous consideration for Fig. 2, because it is much smaller than waves passing through the up arm. In the vicinity of the resonance at a narrow peak at  $E_n$ , we have

$$\begin{aligned} t_{jj'}^d &\approx -2\pi i D(E) \left[ \frac{V_{jn}V_{nj'}}{E - E_n + i\Gamma_n} + \frac{V_{jN}V_{Nj'}}{E_n - E_N} \right] \\ &= -2\pi i D(E) \frac{V_{jN}V_{Nj'}}{E_n - E_N} \left( \frac{|(N|\hat{H}'|n)|^2}{(E_n - E_N)(E - E_n + i\Gamma_n)} + 1 \right). \end{aligned} \quad (15)$$

This shows that the Fano interference of the resonance at  $E_n$  with the nonresonant transmission through the dot state  $E_N$

changes sign when the energy crosses  $E_N$ , i.e.,  $q' < 0$  and  $q' > 0$  in the left- and right-hand side, respectively.

Figure 5 shows the calculated conductance when the up arm is pinched off with  $V_c/E_F = 2$ . The conductance averaged over a finite width of the gate potential is also included, which shows only the structure due to broad peaks because narrow peaks are all averaged out. For the narrow peaks, we see the Fano line shape with a dip. In the vicinity of a wide peak, the asymmetry of narrow peaks is such that  $q' < 0$  in the left-hand side and  $q' > 0$  in the right-hand side, in agreement with the above simple approximation [Eq. (15)].

Figure 6 shows the phase of  $t_{22}$  which makes a dominant contribution to the conductance. The phase changes by  $\sim \pm \pi$  when the gate potential crosses each wide peak following essentially the dotted line, but not at narrow peaks. In a one-dimension system with a single dot, the Friedel sum rule requires the phase change of  $\pi$  whenever the energy crosses a dot state, unless same parity states are in sequence.<sup>16</sup> Therefore, the phase change across each wide peak is reasonable, because wide peaks correspond to dot states associated with the lowest 1D subband contributing to the tunneling.

#### IV. DEPENDENCE ON CONTROL GATE

Figure 7 shows a whole picture of the calculated conductance as a function of the gate potential and the control gate

for the magnetic field  $\phi/\phi_0=79.9$ . The conductance when the down arm is pinched off is shown by a thick solid line in the  $G$  vs  $V_c$  plane. It is essentially the same as the off-resonance conductance in the presence of the quantum dot. With the decrease of the control gate, the channels are opened one by one, leading to conductance steps with a small oscillation due to a Fabry-Perot type interference.

Many asymmetric peaks due to the interference with states in the dot are superposed on the off-resonance conductance. The contribution of this current through dot states oscillates with the control gate considerably and depends also on the gate potential in the dot, i.e., on dot states. This is presumably results of complex interferences in the AB ring. An extreme example was demonstrated in one-dimensional model without a control gate, in which only dot states with the same parity can contribute to the conductance.<sup>13</sup>

Blowups of the region in the vicinity of a wide peak at  $V_g/E_F \sim -0.06$  and at  $V_g/E_F \sim 0.07$  are shown in Fig. 8. The two wide peaks shown in the figure are adjacent to each other and their asymmetry is opposite when  $V_c/E_F=1$ . We note first that the contribution of dot states is largest in the case where the control gate is close to the pinch-off and becomes much smaller when the channel in the up arm is well open. This can be understood classically as follows: The total current through the AB ring is limited by the ideal lead, i.e., by a quantum point contact between the AB ring and a two-dimensional system. Therefore, when the up arm is opened up, most of the current tends to go through the up arm, reducing the current through the down arm.

As a function of the control gate the asymmetry of the peaks changes in a quasiperiodic manner due to interferences inside the AB ring. At certain control gates, for example, at  $V_c/E_F=0.68$  as shown in a dotted line, the asymmetry of adjacent wide peaks become the same. Such an exception seems to appear when the contribution of these dot states to the current becomes considerably small. The rule that asymmetry of narrow peaks follows that of a nearest wide peak is largely valid for arbitrary values of the control gate. However, a close examination of Fig. 8 reveals that exceptions appear sometimes particularly when the amplitude of the wide peak is small.

The asymmetry of wide peaks becomes more complicated when several channels contribute to the current for small values of the control gate. An example is shown in Fig. 9 for  $V_c/E_F=0.1$ , where two channels can pass through the up arm. All peaks have a dip in the right side in this example. Even in this extreme case, the rule that asymmetry of narrow peaks follows that of a nearest wide peak remains still valid.

## V. DISCUSSION

In actual experiments, as the charging energy of a dot is dominant, it causes a Coulomb blockade effect and determines a typical scale of the gate potential. As has been shown in the above-mentioned examples, most of the dot states contributing to the Coulomb oscillation are those of

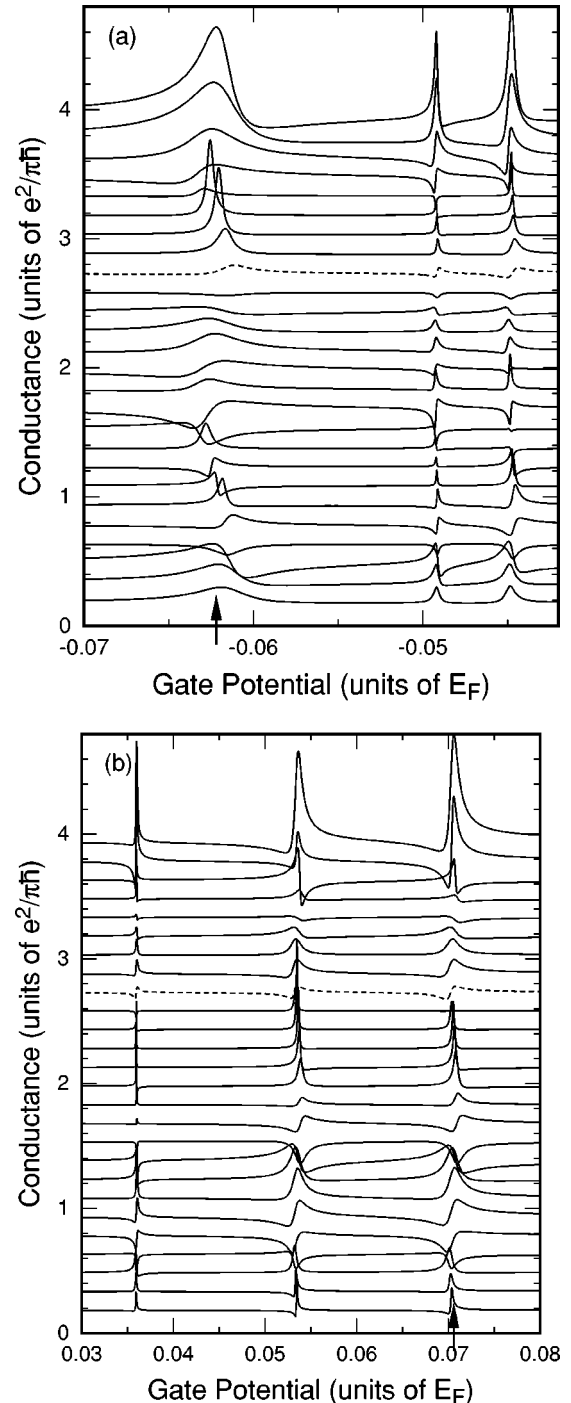


FIG. 8. The dependence on the control gate around wide peaks at (a)  $V_g/E_F = -0.06$  and (b)  $V_g/E_F = 0.07$  pointed by arrows. The control gate is shifted at regular intervals of  $0.04E_F$  from the bottom curve for  $V_c/E_F=0$  to the top one for  $V_c/E_F=1$ . The origin of the vertical axis is shifted consecutively.

narrow peaks because of their dominance in the number and only a few of those of wide peaks appear. This means that the asymmetry of the Fano resonance stays the same for several consecutive narrow conductance peaks as long as they are connected with the same wide peak [Eq. (13)] and also the phase of the AB oscillation does not change among such peaks.

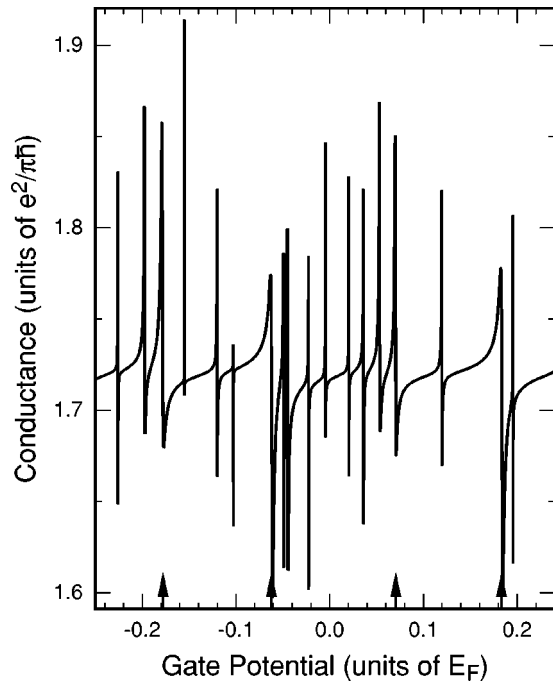


FIG. 9. Calculated conductance for open control gate  $V_c/E_F = 0.1$  and magnetic flux  $\phi/\phi_0 = 79.9$ . The arrows indicate the position of the wide peaks when the up arm is pinched off.

The asymmetry of a narrow peak changes, when the dot state contributing to the narrow peak is mixed to a different dominant wide-peak state. In the region of such crossover gate potential, the asymmetry may exhibit a complicated behavior because a dominant wide-peak state may vary from peak to peak. Further, the phase of the AB oscillation changes only when the gate potential crosses the wide peak. These behaviors can account for most of the features of the experimental results [Fig. 2(a) of Ref. 1, for example].

There remains a slight disagreement with experiments.<sup>1,2</sup> Experimentally the phase of the AB oscillation under off-resonant conditions seems to vary slowly as a function of the gate potential [see Fig. 4(c) of Ref. 1, for example], while the present results give almost a constant phase independent of the gate potential as shown in Fig. 2. This is likely to originate from the simplified model of the symmetric gate potential in the present calculation, in which the gate changes energy levels but not the wave function in the dot. In actual experiments using a side-gate structure, the gate potential modifies the form of the dot and is likely to change the phase of the transmission coefficient through the dot due to the gate-potential dependence of  $V_{jN}V_{Nj'}$  in

$$t_{jj'}^d \approx -2\pi i D(E) \frac{V_{jN}V_{Nj'}}{E - E_N}, \quad (16)$$

leading to a phase change of the AB oscillation. The present model is useful for clarifying global features of Fano interferences in an AB ring with a dot, however.

In the absence of a random potential, the result is qualitatively the same as the results given above with a

few exceptions on the asymmetry of the Fano resonance of narrow peaks. Without randomness, the dot is symmetric and therefore the symmetry of the wave function can play important roles in causing mixing between dot levels. In fact, the exception can appear more easily, if the symmetry of wave function prevents a narrow level from coupling to a nearest wide level but allows to a different wide level.

## VI. SUMMARY AND CONCLUSION

We have numerically calculated the conductance using a realistic model of an AB ring with a quantum dot in a down arm and a control gate in the up arm which controls the channel number. Many peaks appear in the conductance, but they can be classified into two groups, small numbers of wide peaks with large broadening and large numbers of narrow peaks. The sign of the asymmetry parameter of the Fano-type interference of narrow peaks is almost always the same as that of a nearest wide peak.

When the control gate is such that the up arm is nearly pinched off, the situation is close to that of double-slit experiments, and therefore the asymmetry parameter changes at the middle of neighboring wide peaks and the phase of the AB oscillation changes by  $\sim \pi$  only when the gate potential crosses the wide peak. With the decrease of the control gate, interference effects in the AB ring become important and the contribution of the current through the dot becomes small and exhibits a Fabry-Perot type oscillation as a function of the control gate. The asymmetry of narrow peaks follows that of a nearest wide peak even in this case.

Most of dot states contributing to the Coulomb oscillation are those of the narrow peaks because of their dominance in the number. Consequently, the asymmetry of the Fano line shape stays the same for the several consecutive narrow conductance peaks as long as they are connected with the same wide peak and also the phase of the AB oscillation does not change among such peaks, which explains essential features of experiments.

*Note added in proof:* After completion of this manuscript, the authors discovered the existence of two papers relevant to the subject, Ref. 24 which provides a mechanism giving rise to the extra  $\pi$  phase change between neighboring peaks in a near chaotic dot and Ref. 25 which discusses effects of lossy channels in the Aharonov-Bohm ring.

## ACKNOWLEDGMENTS

We thank K. Kobayashi, S. Katsumoto, and Y. Asai for helpful discussion. This work has been supported in part by a 21st Century COE Program at TokyoTech “Nanometer-Scale Quantum Physics” and by Grant-in-Aid for COE (12CE2004 “Control of Electrons by Quantum Dot Structures and Its Application to Advanced Electronics”) from the Ministry of Education, Science and Culture, Japan. Numerical calculations were performed in part using the facilities of the Supercomputer Center, Institute for Solid State Physics, University of Tokyo and of TACC, AIST.

- <sup>1</sup>K. Kobayashi, H. Aikawa, S. Katsumoto, and Y. Iye, *Phys. Rev. Lett.* **88**, 256806 (2002).
- <sup>2</sup>K. Kobayashi, H. Aikawa, S. Katsumoto, and Y. Iye, *Phys. Rev. B* **68**, 235304 (2003).
- <sup>3</sup>J. Göres, D. Goldhaber-Gordon, S. Heemeyer, and M.A. Kastner, *Phys. Rev. B* **62**, 2188 (2000).
- <sup>4</sup>I.G. Zacharia, D. Goldhaber-Gordon, G. Granger, M.A. Kastner, Yu.B. Khavin, H. Shtrikman, D. Mahalu, and U. Meirav, *Phys. Rev. B* **64**, 155311 (2001).
- <sup>5</sup>U. Fano, *Phys. Rev.* **124**, 1866 (1961).
- <sup>6</sup>A. Shibatani and Y. Toyozawa, *J. Phys. Soc. Jpn.* **25**, 335 (1968).
- <sup>7</sup>K. Terakura, *J. Phys. F: Met. Phys.* **7**, 1773 (1977).
- <sup>8</sup>A. Yacoby, M. Heiblum, D. Mahalu, and H. Shtrikman, *Phys. Rev. Lett.* **74**, 4047 (1995).
- <sup>9</sup>A. Yacoby, R. Schuster, and M. Heiblum, *Phys. Rev. B* **53**, 9583 (1996).
- <sup>10</sup>R. Schuster, E. Buks, M. Heiblum, D. Mahalu, V. Umansky, and H. Shtrikman, *Nature (London)* **385**, 417 (1997).
- <sup>11</sup>Y. Gefen, Y. Imry, and M.Ya. Azbel, *Phys. Rev. Lett.* **52**, 129 (1984).
- <sup>12</sup>A.L. Yeyati and M. Büttiker, *Phys. Rev. B* **52**, R14 360 (1995).
- <sup>13</sup>J. Wu, B.-L. Gu, H. Chen, W. Duan, and Y. Kawazoe, *Phys. Rev. Lett.* **80**, 1952 (1998).
- <sup>14</sup>H. Xu and W. Sheng, *Phys. Rev. B* **57**, 11 903 (1998).
- <sup>15</sup>C.-M. Ryu and S.Y. Cho, *Phys. Rev. B* **58**, 3572 (1998).
- <sup>16</sup>H.-W. Lee, *Phys. Rev. Lett.* **82**, 2358 (1999).
- <sup>17</sup>O. Entin-Wohlman, A. Aharony, Y. Imry, Y. Levinson, and A. Schiller, *Phys. Rev. Lett.* **88**, 166801 (2002).
- <sup>18</sup>A. Ueda, I. Baba, K. Suzuki, and M. Eto, *Suppl. A to J. Phys. Soc. Jpn.* **72**, 157 (2003).
- <sup>19</sup>T. Nakanishi and T. Ando, *Phys. Rev. B* **54**, 8021 (1996); *Physica B* **227**, 127 (1996).
- <sup>20</sup>A. Kumar, S.E. Laux, and F. Stern, *Phys. Rev. B* **42**, 5166 (1990).
- <sup>21</sup>T. Suzuki and T. Ando, *J. Phys. Soc. Jpn.* **62**, 2986 (1993).
- <sup>22</sup>R. Landauer, *IBM J. Res. Dev.* **1**, 223 (1957); *Philos. Mag.* **21**, 863 (1970).
- <sup>23</sup>T. Ando, *Phys. Rev. B* **44**, 8017 (1991).
- <sup>24</sup>P.G. Silvestrov and Y. Imry, *Phys. Rev. Lett.* **85**, 2565 (2000).
- <sup>25</sup>A. Aharony, O. Entin-Wohlman, B.I. Halperin, and Y. Imry, *Phys. Rev. B* **66**, 115311 (2002).